applied sciences

MDPI

Article

Reveal of Internal, Early-Load Interfacial Debonding on Cement Textile-Reinforced Sandwich Insulated Panels

Eleni Tsangouri *, Hasan Ismail, Matthias De Munck, Dimitrios G. Aggelis and Tine Tysmans

Department Mechanics of Materials and Constructions (MeMC), Vrije Universiteit Brussel (VUB), 1050 Ixelles, Belgium; Hasan.Ismail@vub.be (H.I.); Matthias.DeMunck@vub.be (M.D.M.); Dimitrios.Aggelis@vub.be (D.G.A.); Tine.Tysmans@vub.be (T.T.)

* Correspondence: Eleni.Tsangouri@vub.be

Abstract: Internal interfacial debonding (IID) phenomena on sandwich façade insulated panels are detected and tracked by acoustic emission (AE). The panels are made of a thin and lightweight cementitious composite skin. In the lab, the panels are tested under incremental bending simulating service loads (i.e., wind). Local (up to 150 mm wide) skin-core detachments are reported in the early loading stage (at 5% of ultimate load) and are extensively investigated in this study, since IID can detrimentally affect the long-term durability of the structural element. A sudden rise in the AE hits rate and a shift in the wave features (i.e., absolute energy, amplitude, rise time) trends indicate the debonding onset. AE source localization, validated by digital image correlation (DIC) principal strains and out-of-plane full-field displacement mapping, proves that early debonding occurs instantly and leads to the onset of cracks in the cementitious skin. At higher load levels, cracking is accompanied by local debonding phenomena, as proven by RA value increases and average frequency drops, a result that extends the state-of-the-art in the fracture assessment of concrete structures (Rilem Technical Committee 212-ACD). Point (LVDT) and full-field (AE/DIC) measurements highlight the need for a continuous and full-field monitoring methodology in order to pinpoint the debonded zones, with the DIC technique accurately reporting surface phenomena while AE offers in-volume damage tracking.

Keywords: sandwich-insulated panel; interfacial debonding; cementitious composite; insulation; fracture; acoustic emission; digital image correlation; out-of-plane displacement; shear mode; cracking

Citation: Tsangouri, E.; Ismail, H.; De Munck, M.; G. Aggelis, D.; Tysmans, T. Reveal of Internal, Early-Load Interfacial Debonding on Cement Textile-Reinforced Sandwich Insulated Panels. *Appl. Sci.* **2021**, *11*, 879. https://doi.org/10.3390/app11020879

Received: 13 December 2020
Accepted: 14 January 2021
Published: 19 January 2021

1. Introduction

The sandwich design is optimal for pre-cast concrete structural elements (floor, roof, wall, façade insulated panels, etc.), since it offers an excellent strength-to-weight ratio and minimum manufacturing costs [1]. Nowadays, the rigid skin phases are cast in textile-reinforced cement (TRC): cementitious mortar reinforced with continuous impregnated textiles that provides bending strength and stiffness [2]. In between the skins, an insulation layer of a low density (typically of foam nature), cast in high thickness contributes to thermal and acoustic isolation and provides flexural rigidity (increase in the moment of inertia) and, in some cases, shear and/or buckling resistance as well [3]. The concept imitates the well-established "I-section" on metal structures, as the skin phases act as the flanges and the core stands for the web [4], however an essential difference should be highlighted. The cementitious composite skin is adhesively bonded to or only cast and deposited on the core; therefore, it is evident that interfacial detachment can occur due to weak joining, a condition that detrimentally affects and potentially puts the sandwich element structural integrity at risk.

The interfacial debonding issue has been investigated since the first ferrocement sandwich insulated panels were designed; at that moment, a wet-on-wet fabrication process was proposed to ensure a good adhesion between the aerated concrete and the ferrocement [5]. Technological advances based on the pioneering contributions of Cuypers [6] and

Hegger [7], among others, led to the establishment of continuous textile reinforcement at the sandwich skin layer [8,9] m and nowadays demonstration projects and several commercial products have been launched and reported great structural performance. Still though, the interfacial bonding remains a bottleneck, as has been extensively discussed in [10]. In that direction, and in an attempt to enhance the mechanical response and ensure a firm core-skin connection, the use of metallic connectors was recommended [11,12]. The nail-type connectors also address the creep issue by compensating for the viscoelastic behavior of the foam core [12]. Indicatively, a glass-fiber polymer connector is designed to interconnect the TRC skins and, under service loads, appears to control the mechanical response of the sandwich elements that eventually fail due to the local connector's pull-out and buckling phenomena [13]. In all study cases, it is evident that interfacial debonding detection and tracking is challenging, first of all because the phenomenon occurs internally, and therefore visual confirmation is not possible. Besides this, manufacturing defects can lead to pre-existing disbands that lead to skin/core debonding under compression [3]/bending [14] service loads. Based on empirical evidence, the surface treatment of the core material can enhance the interfacial adhesion and ensure the optimal response of the core under loads—namely, shear failure [15]. In a recent study, it was shown that the core material's nature dominates the sandwich response to flexure. In detail, EPS (expanded polystyrene) and XPS (extruded polystyrene) insulation cores were considered for the design of wall insulated panels, where progressive interfacial debonding was detected only in the case of the weaker XPS core [16]. The urgent need to assess the conditions under which this defect occurs has attracted the attention of the research community, since interfacial debonding can lead to a drop in the sandwich ultimate strength [16], but also it serves as a conduit that allows access to heat [17] or air entrapment [18].

Conventional methods for debonding detection, such as CT scans and X-ray scans, are cost-ineffective and limited to small-scale point-by-point inspections, therefore they cannot be considered for real-size sandwich-insulated panel evaluation [19]. Guided wave inspection is gaining popularity in the field: among others, a laser Doppler vibrometer was used to emit low-frequency guided waves [20]. It was shown that the wave mode shifted to antisymmetric Lamb wave in the presence of debonding. Song et al. developed a multi-level network of actuator-receiver sensors and used leaky guided waves to detect and measure the size of multiple debonded zones [19]. It is worth highlighting the fact the complex image fusion methodology that is required to superimpose point measurements and reconstruct the debonded zones. The latter disadvantage led to the proposal of an alternative wave-based methodology in this study—namely, passive Acoustic Emission inspection.

Acoustic emission (AE) has a long-history in the monitoring of delamination phenomena in concrete structural elements retrofitted with fiber-reinforced external layering [21]. In a pioneering study, Yoon et al. correlated the delaminations at high load levels with the release of high-magnitude AE [22]. Carpinteri et al. defined the delamination onset based on AE b-value analysis and tracked the fracture snap-back instability by AE localized event distribution [23]. Interfacial debonding onset and propagation on hybrid concrete hollow TRC beams has been effectively reported by Aggelis et al. by following the shift in the AE hits rate, the active AE events source location, and the changes in AE wave features [24,25]. Nowadays, AE wave features shift (i.e., rise time jump in values as the stress is released in debonded zones) has been established as a damage indicator to discriminate fiber reinforcement delamination and pull-out from other synchronous-active damage modes (i.e., concrete cracking, steel rebars plastic deformation, etc.) [26]. In a similar study, Gallego et al. reported AE hits of a longer duration and lower amplitude as the pull-out of the concrete reinforcement evolves and slipping leads to the wearing of the interface surface [27]. To summarize, the extended literature on the application of AE as a debonding/delamination indicator has shown that:

- The AE intensity and signal strength indicate the transition from matrix micro-cracking to the reinforcement debonding onset [26], and beyond that moment AE

intensity rise tracks the progressive debonding stages (i.e., adhesion, friction, mechanical interlocking) [28].
- The AE wave features that describe the early part of the waveform, such as the rise time (RT) and the RA value, can indicate the presence of shear-dominated debonding actions [29].
- The shifts in the frequency range can be an indication of interfacial debonding and slippage, however no confident pattern has been reported among the different frequency indices (initiation/average/peak frequency) [22,30].

In this paper, a comparative study is performed between a *reference* (REF) sandwich-insulated panel and one at which early AE activity is proven to occur due to *internal* skin-core *interfacial debonding* (IID). The panels are manufactured in an identical way and tested in incremental bending, simulating in-service wind loads. AE continuously monitors the damage progress and the findings fully characterize the interfacial debonding. Digital Image Correlation (DIC), a full-field optical inspection technique, is applied to validate the AE observations and to provide complementary evidence of debonding. In the literature, DIC out-of-plane displacement tracking has been effectively applied in the work of Vervloet et al. to detect the buckling of thin-walled TRC-skin sandwich-insulated panels under compression [31]. Fathi et al. measured the shear deformation of different foam materials designed as core elements on sandwich panels tested in bending [32]. For the first time in the literature, an integrated inspection methodology combines the AE and DIC outcome, localizes and measures the premature interfacial debonding, and also distinguishes this detrimental effect from other damage sources (i.e., cracking, pull-out).

The detection of premature interfacial debonding appears to be of utmost importance for the structure's integrity and long-term durability. In this direction and for the first time in the literature to the best of the authors' knowledge, this study provides an integrated monitoring methodology and an essential tool for the continuous and full-field tracking of the damage progress.

2. Materials and Methods

2.1. Materials

As illustrated in Figure 1a, a series of panels of 2.5 m width and 2.5 m length were cast with a thickness of 0.21 m. The materials used and the manufacturing and casting process were identical for all the prepared samples. The core was made of EPS (expanded polystyrene). EPS insulation material was selected due to its relatively high density (that ensures endurance) and its cost-effectiveness. The core thickness was set to 0.2 m to ensure sufficient compressive/shear strength and insulation efficiency [33].

The cover skins were made of textile-reinforced cement (TRC). The TRC mechanical properties were obtained by means of numerous tensile coupon tests (150+ samples) and sandwich beam bending tests (50+ samples), at which a limited variability on the fracture response is obtained.

No connectors were added to enhance the skin–core bonding. First, a TRC skin was cast on top of the EPS core. The cement-polymer mortar (KLEEFSTOF TM 282, provided by Tillman BVBA) was poured and, following this, a layer of glass textile (geometry given in Figure 1a) was impregnated with the hand-layup method in the mortar layer using a de-airing roller [33]. The textile was fully covered with extra mortar added on top, reaching eventually a total thickness of 5 mm. The cover thickness was controlled by passing a wet steel beam along the top of the mold after casting (Figure 1b). The first core layer was protected with plastic sheets and left to cure for 7 days in ambient conditions (Figure 1c). Afterwards, the panel was manually flipped and the second layer of the TRC was cast likewise. The sandwich structure was further cured for 28 days in ambient conditions. The material properties are reported in Table 1 and extensively in [34].

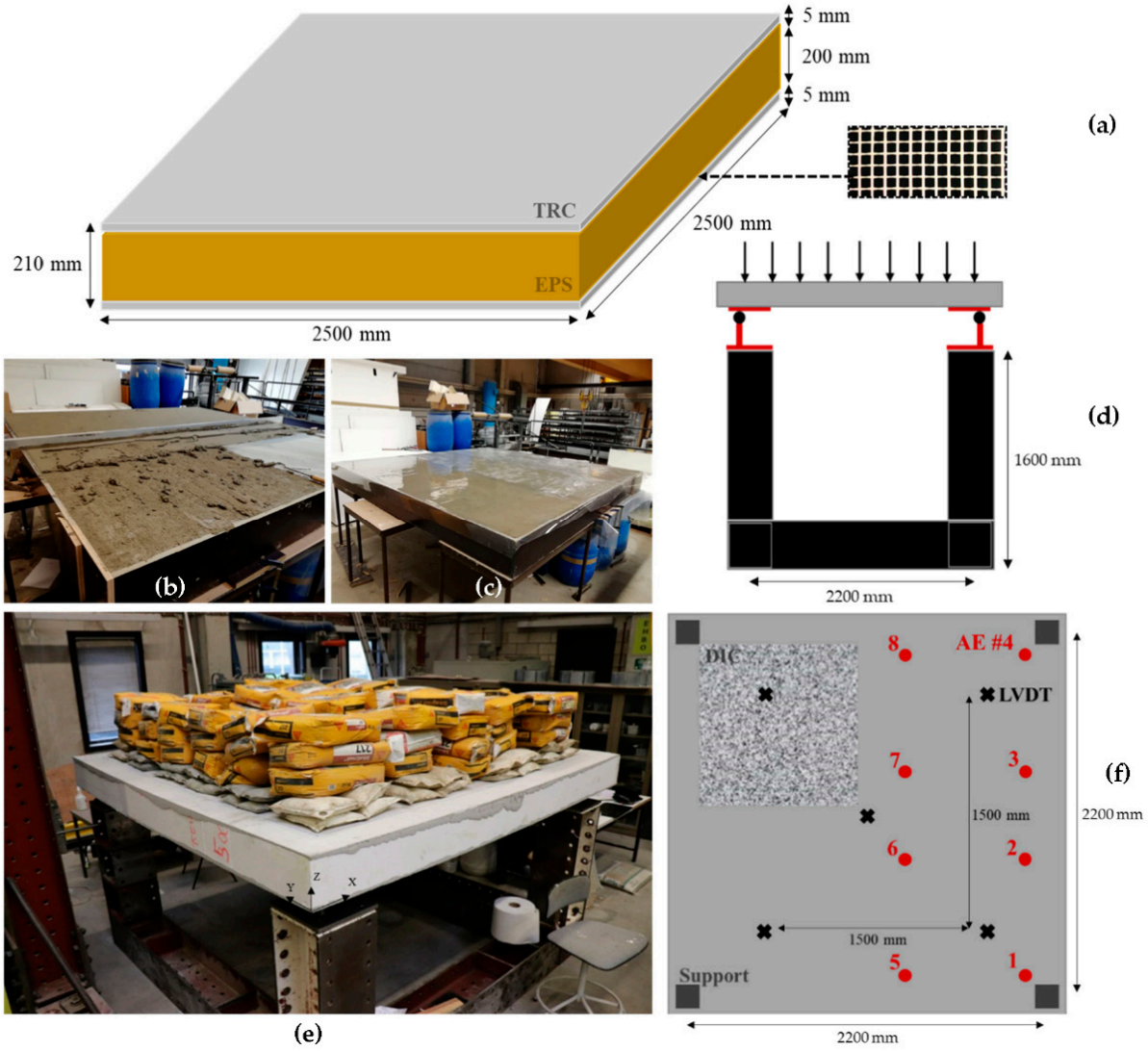

Figure 1. Sandwich-insulated panel: (**a**) specimen geometry and detail of the textiles' geometry; (**b**) a wet steel beam is passed along the top of the mold to control the panel's thickness; (**c**) the core layer is covered with a plastic sheet after casting; (**d**) loading support and setup; (**e**) the panel under load. Sand and cement bags are symmetrically distributed at the top skin of the panel. (**f**) Drawing of the bottom view: the Digital Image Correlation area of interest is marked with a speckle pattern, the AE sensors' position is marked in red, and the Linear Variable Differential Transformer (LVDT) sensors are marked in black.

Table 1. Material properties.

Fine-Grained Organic Portland Cement		**2D Alkali Resistant-Glass Textile**		**EPS (Expanded Polystyrene) Core**	
Vws Polystyreen Kleefstof TM282		**Woven in Orthogonal Mesh**		**Density (kg/m^3)**	**27**
Water/binder	0.125	Polymer-based yarn coating		Compressive strength (MPa)	10
Density (kg/m^3)	1754	Tensile strength (N/50 mm)	2500	Flexural strength (kPa)	250
Flexural strength (MPa)	4.96	Total surface weight (g/m^2)	200	Shear strength (kPa)	125
Tensile strength (MPa)	2.18	Mesh opening (mm)	5	Elastic modulus (MPa)	9.3
Compressive strength (MPa)	29.6	Max. sheet width (mm)	1000	Poisson ratio	0.12

2.2. Loading

During testing, the sandwich-insulated panel was placed on a support metal frame and the supported area is equal to 2.2 m to 2.2 m (Figure 1d,e). On top of the metal frame blocks, a metal ball was fixed on low-friction sockets at each corner of the panel. An extra metal plate (0.2 m × 0.2 m × 15 mm) with a gap that fits to the metal ball to ensure rotational

support was added and finally, the panel was placed on top of an extra layer of rubber plate (0.2 m × 0.2 m × 15 mm) [34]. The sandwich-insulated panel was designed to be used as a façade structural element, therefore the mechanical performance was tested simulating the load of wind pressure. For reasons of simplification, the study does not consider the effect of connections' capacity on the panels' mechanical performance, therefore the extreme loading condition of wind suction is not investigated. It is worth mentioning that the experimental outcome is taken into account for the validation and calibration of an extensive numerical FEM study that investigates different load combinations [34].

A distributed load was applied at the top skin of the sandwich-insulated panel by placing sand and cement bags that were incrementally and carefully placed covering the supported zone (2.2 m × 2.2 m). The loading process did not interfere with the test result, as verified by the absence of noise in the AE data. The uniformly distributed load was measured and normalized relative to the top surface area in kN/m^2. At each loading cycle set at 0.5 kN/m^2, the deflection was measured using LVDT devices set at the supporting zones and the center of the panel (see Figure 1f) and a DIC picture was captured. At the end of each loading cycle, a loading pause of 8 min was performed. The inspection with AE and DIC stops as the load of 5 kN/m^2 was reached. Beyond that stage, the deflection was significant, the crack saturation point was reached, and instant collapse could have occurred at any moment, therefore both the AE and DIC hardware were removed. The failure load was measured up to 10 kN/m^2; at that load level, the bottom TRC skin instantly fails in tension and the core catastrophically breaks in two pieces due to shear.

2.3. Acoustic Emission

In total, eight AE sensors were mounted at the bottom TRC skin in a configuration illustrated in Figure 1d (red-colored spots). Vaseline was used to ensure the optimal surface contact with the TRC, and the sensors were supported by a magnetic holder. Resonant R15 sensors (150 kHz) were provided by Physical Acoustics and connected to a 40 dB pre-amplification system. AE continuously monitored the damage activity, both at the loading and pausing cycles, and the time periods corresponding to each loading cycle were manually tracked. The AE data were collected and stored by the AEwin software and post-processed by the Noesis software. The amplitude threshold was set at 35 dB, a value fixed considering ambient noise and vibrations/sounds from the deposition of the bags. Wave source planar localization was based on the triangulation algorithms of the AEwin software. Due to the limited TRC thickness, the in-depth accuracy of the localization analysis was questioned, and therefore the AE events were projected in a planar view covering half of the TRC bottom side. The TRC wave propagation velocity was measured at the intact stage, averaging at 3000 m/s. Further details on the AE setup are given in Table 2.

Table 2. AE setup details.

Transducer	R15	AE Device	PAC micro-8
Sampling rate	2 MHz	Pre-amplification	40 dB
Sampling frequency range	10 kHz–2 MHz	Wave velocity (m/s)	3000
Threshold	35 dB	Event lock-out value (mm)	2000

2.4. Digital Image Correlation

A pair of high-definition cameras were installed at the base of the testing frame. The cameras were positioned along a stabilizer beam to ensure that no movement occurs during testing. The DIC area of interest (AOI) was limited to a quartile of the panel, assuming a symmetric response along the length and width of the panel. Optical lenses of 21 mm focal length were mounted on the cameras. A stereo-scopic calibration of the system was performed before testing. Pairs of synchronized images were captured and stored using the VIC-Snap software. The images were post-processed using the VIC-3D software provided by Correlated Solutions. Further details on the DIC setup are listed in Table 3.

A measurement was taken after the load placement at each loading cycle. The reference image was considered the one taken at the intact state before loading started. In the Results section of this paper, the principal strain E1 was selected to be discussed, since it provides a clear mapping of cracks considering the strain distribution in both X and Y directions. Additionally, the out-of-plane displacement (W) in the Z direction was plotted to track the interfacial debonding of the TRC skin. It was noted that the panel rigid body motion was removed (post-testing correlation function of the VIC 3D software) to ensure that only the deformation of the TRC skin was measured.

Table 3. DIC setup details.

Camera Resolution (Pixels)	2564 × 2048	Strain Window Size (Pixels)	9
Spatial sensitivity (mm/pixels)	0.15	Capturing software	VIC-Snap
Subset/Step (pixels)	21/7	Post-procession	VIC-3D

3. Results

3.1. REF Versus IID: First Evidence of Different Damage Progress

As previously mentioned, a comparative analysis will follow between a REF panel and one that carries unexpected early AE activity hypothesized to be related to skin-core interfacial debonding (IID). It should be noted that in total three panels were tested; in two of them, IID failure was reported.

In Figure 2, an overview of the loading process for both series is given. An incremental increase in the loading in time is projected together with the scatter plot of the AE hits absolute energy. The AE energy was proven to be a descriptor of fracture energy accumulation [35,36], but it can also indicate the transition from early micro-cracking to severe crack formation or other internal fracturing [29]. At the early loading stage, sporadic AE activity of low energy is reported for both samples under study. However, a burst in AE energy values was already monitored for the IID series at 0.5 and 1.5 kN/m^2. As the load increased, several additional jumps in the AE energy were captured mainly at the active loading stage (not in the course of the load pause). The same AE feature trends evolved until reaching 5 kN/m^2. In contrast, for the REF panel there was limited AE activity of negligible energy until the load of 3.5 kN/m^2. Beyond that point and likewise in the IID case, the AE hits that were continuously emitted carried many significant bursts of energy.

In Figure 2c, the cumulative graph of AE hits population at incremental loading illustrates that not only the was AE energy high for the IID series very early, but also that the number of hits was much greater for the IID series at this early loading stage. Indicatively, at 3.5 kN/m^2 the hits emitted at the REF panel were limited to 2263 and the respective hits number in the IID case was up to 14010.

At the next step, the AE sources related to specific damage modes were assessed considering the wave rise time (RT) and the frequency distributions, since the established literature demonstrates that RT rises and frequency drops as the shear becomes dominant in the presence of debonding/detachment phenomena [29]. The time periods of the burst AE energy activity are isolated, and a representative sampling of each series is demonstrated in Figure 3. As expected, the RT reaches a maximum and the initiation frequency (IF) a minimum at the moment where numerous hits of high energy were emitted, a result that validates the presence of shear-dominated damage, either due to internal TRC skin failure or skin-core interfacial detachment.

3.2. Focusing on Damage Onset and Propagation

In Figure 4, the DIC principal (E1) strains maps visualize the surface cracks formed on the TRC skin under bending. The cracks were identified by tracking the zones of relatively high displacement at both crack fonts, which were therefore of high strain concentration (color ruler added in Figure 4 to indicate the strain magnitude) compared to the rest of the panel, where the strain remained negligible (marked with purple color). The principal strains E1 were selected since they highlight the dominant damage phenomena at the panel

surface and were obtained as the critical combination of maximum normal strains along the length and the width of the panel.

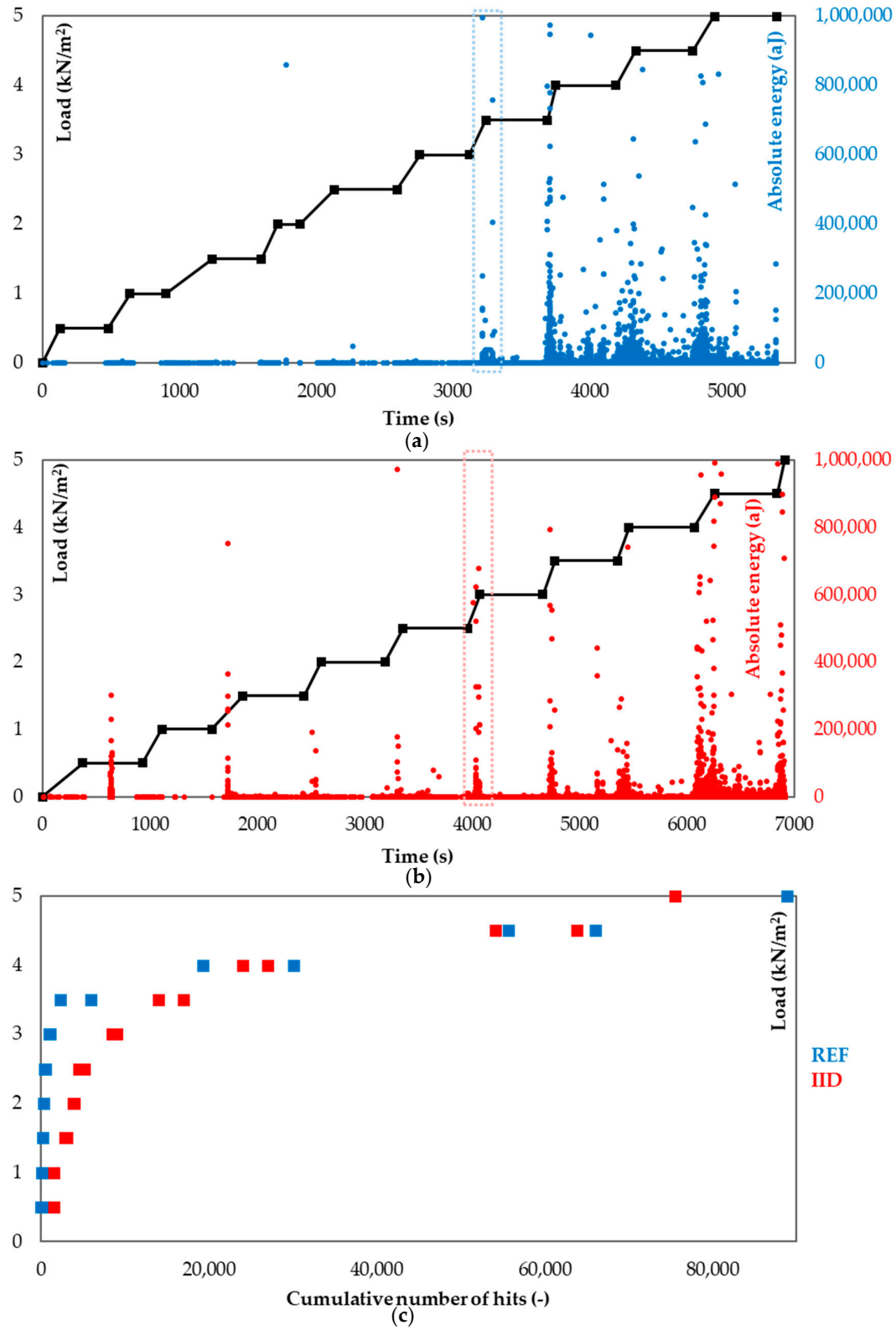

Figure 2. AE hits analysis: load and absolute energy plots in time for (**a**) Reference (REF) and (**b**) Internal Interfacial Debonding (IID) panels; (**c**) cumulative plot of the hit population for both test cases. Incremental loading step of 0.5 kN/m^2.

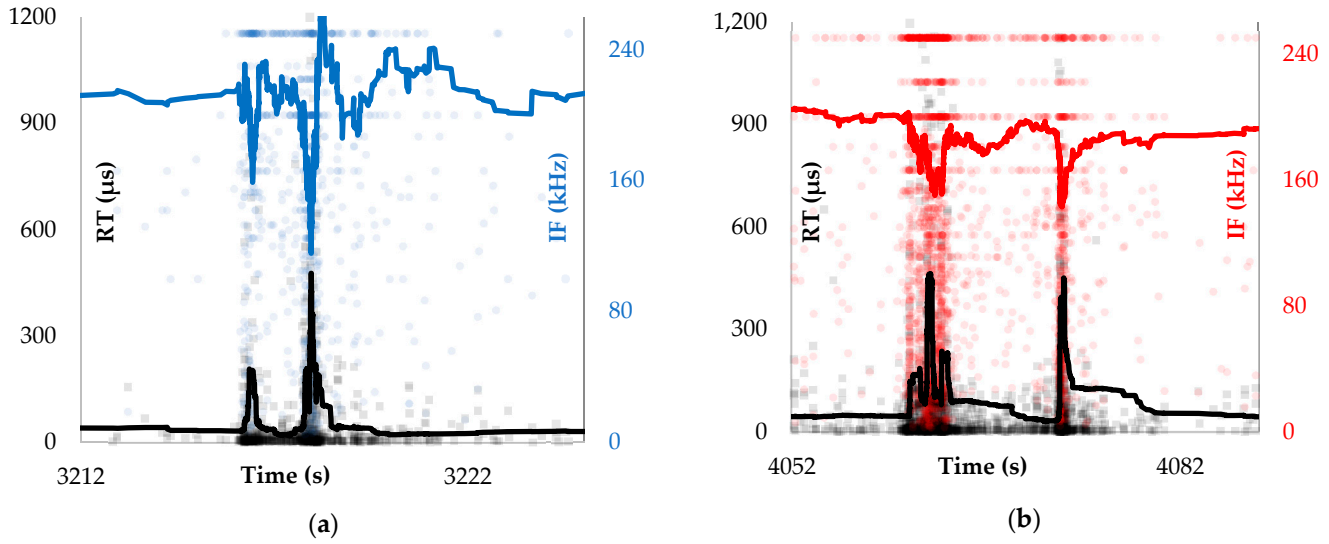

Figure 3. Rise time (RT) and Initiation frequency (IF) scatter plots (data in transparent font) for a representative time period (marked in Figure 2a,b) of a jump in AE energy. Averaging (each 250 points) trend line is plotted for (**a**) REF and (**b**) IID panels.

Several micro-cracks formed as early as at 0.5 kN/m^2 (E1 strain measured not negligible, marked in circle in Figure 4) and extensively propagated, leading to the formation of the first macro-crack at 1.5 kN/m^2 in the IID case. This means that early high AE energy values are sourced from a combination of debonding and cracking. It is speculated that interfacial debonding leads to crack formation or that cracking leads to TRC internal debonding. However, since these two phenomena were overlapping, this new information cannot clarify the sequence of events.

On the other hand, and as expected, a series of cracks nucleated for the REF panel only after the AE energy jumped at 3.5 kN/m^2; at that moment, several zones of strain E1 concentrations were marked throughout the panel's bottom side. As the loading increased, more cracks form and the cracks' density increased, as proven by the extended zones of high E1 strain concentrations. At the end of the monitoring period (at 5 kN/m^2), it is believed that crack saturation was reached, and beyond that point only the textiles resisted further loading. By observing the cracks' distribution and density at that load level (bottom images in Figure 4), it was concluded that potential early debonding appears to have no impact on the cracking pattern.

3.3. Out-of-Plane Deflection Validation of Interfacial Debonding

The out-of-plane displacement was tracked by DIC and proved that the movement in the Z direction was greater for the IID panel at early load level as interfacial detachment occurred. As illustrated in Figure 5a, the out-of-plane displacement was not homogenous throughout the panel bottom side and there were zones with greater displacement as the load increased. The greatest displacement values were detected in both cases in the middle of the AOI. The extensively debonded zones are colored in red and their shape defines the potentially debonded zones under the TRC skin. Indicatively, at 3.5 kN/m^2 extended red zones of great displacement were detected for the IID case compared to the limited red zones for the REF panel. A point was fixed for both series at the zone of the maximum displacement, and the respective displacement is tracked in Figure 5b. A jump in displacement values was detected at 1.5 kN/m^2 for the IID sample, which is direct evidence of out-of-plane movement that can only be associated with interfacial debonding. Quantitatively, the out-of-plane deformation was limited to 95 µm due to the fact that the TRC layer was restricted and under load, therefore the skin cannot freely move. In any case, the inspection guided by AE wave features trends and validated by DIC

displacement mapping defined the moment at which debonding was physically there, and it is remarkable that it occurred so prematurely.

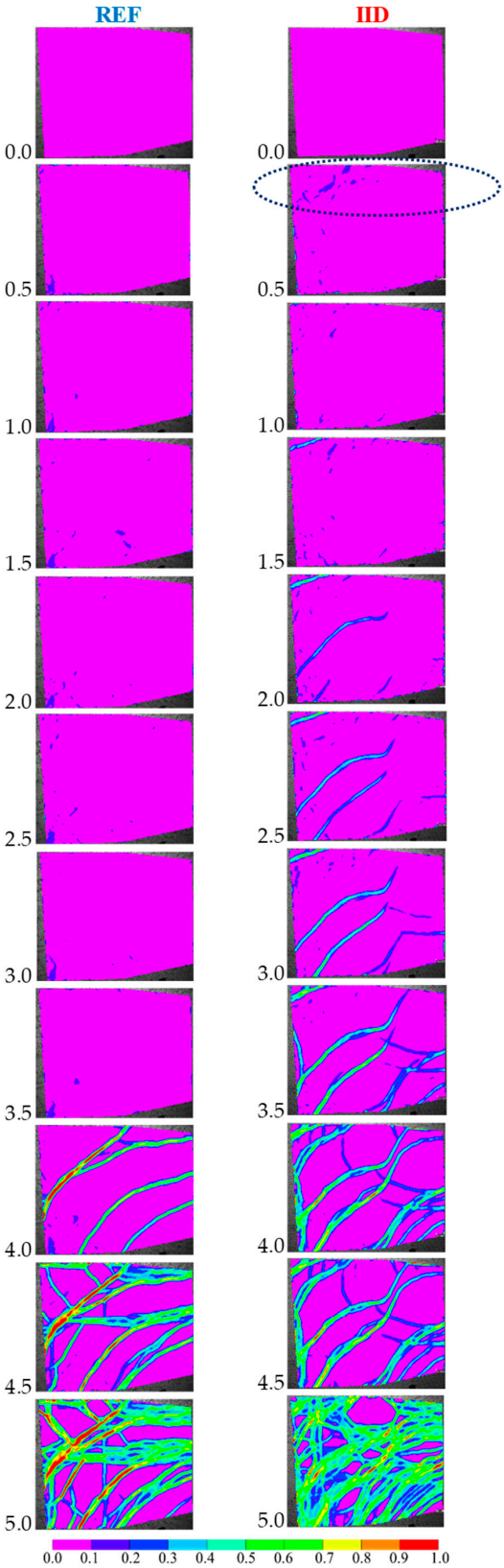

Figure 4. Principal E1 (%) strain maps at each step (in kN/m^2) of incremental load for REF and IID panels.

To validate the presence of local debonding, an extra line was plotted diagonally along the AOI and the displacement distribution along the line is plotted in Figure 5c. In the prior work of Vervloet et al., a similar analysis protocol was adopted to demonstrate how the respective panels tilt under compressive loads [31], thus this work aims to validate the previous work and verify the tool efficacy. Compared to the random and limited fluctuations of the REF line, a clear jump in the displacement values along the IID series line was spotted at the middle zone (across the red colored area in Figure 5a). It is shown that the interfacial debonding is very local and limited to the size of 150 mm. Regarding the pre-debonding AE high-energy/RT activity, it is now evident that the damage was accumulated in the micro-scale level before the instant of detachment. From this perspective, AE feature analysis predicts the premature debonding onset and, in this way, contributes as an alarm method for avoiding this detrimental effect.

3.4. Discussion

At the following paragraphs, the AE and DIC full-field inspection is compared to traditional damage tracking methods and the importance of continuous inspection is highlighted in an attempt to develop an integrated structural health monitoring tool that will detect the potential premature failure of sandwich insulated panels. This aims to improve the panel design and manufacturing process, as well as building the confidence needed to establish this novel structural element for site applications. The analysis proves that AE appears to be a great inspection tool candidate.

3.4.1. Point vs. Full-Field Measurements

As mentioned in Section 2.2, LVDTs were fixed at the center of the panel and at the four panel corners to track the deflection of the element. The central LVDT stands a few millimeters further from the point defined at the DIC map as *Pmiddle* (see Figure 5a). The LVDT and DIC measurements were proven to be identical if the rigid body motion of the panel is excluded. However, in this section, the limited information derived from the point measurements, such as of the LVDT or of the *DIC Pmiddle* point, should be discussed. In Figure 5d, the out-of-plane displacement (rigid body motion excluded) at each loading step for the *Pmiddle* points at both the REF (blue) and IID (red) is projected. It is shown that the out-of-plane displacement is almost identical for the REF and the IID case, therefore by measuring only at a random point in the middle of the panel one cannot detect the local debonding that occurs aside. In other words, point measurements are not capable of detecting a stochastic premature debonding failure, since the debonding onset location cannot be predicted. Therefore, the essential need for full-field inspection methods, such as AE and DIC, is evident. Only by monitoring the whole area under investigation can one pinpoint local debonding that only locally and stochastically occurs.

3.4.2. Effect of Debonding on the Global Failure

Apart from the impact on the long-term durability, the potential effect of premature interfacial debonding on the damage progress should also be considered. The reader is reminded that AE and DIC inspection is limited to 50% of the ultimate load of the panels, therefore the total AE hits activity and DIC displacement at half of the ultimate load are comparatively discussed. Based on Figure 2c, the total number of AE hits stands at the same range for both panels, although the REF panel has 14% more hits than the IID one, a difference that can be neglected, considering the complex fracture progress. Additionally, it is evident that the damage mode does not change; in both cases, the crack saturation point is reached, and the textiles actively resist failure occurring at about 10 kN/m^2. At half of the ultimate load, both panels are fully cracked and, as shown in Figure 5e, their out-of-plane displacement of the bottom skin is identical. The displacement tracking along a diagonal line that crosses the previously debonded zone proves that at higher load levels and at crack saturation level debonding and cracking occur simultaneously, and the structure compensates and adjusts, leading to a homogeneous strain distribution (red zone

Figure 5a at 5 kN/m^2). It is concluded that the ultimate failure is identical for both samples (catastrophic tensile failure of the bottom TRC skin and shear failure of the insulation core at approximately 10 kN/m^2). However, it should be noted that in service, and due to weathering conditions, the water/humidity invasion through the debonded interface at the early load stage can potentially enhance the autogenous sealing at the TRC matrix or, on the contrary, additionally degrade the TRC–core interface due to debonding extension. Future research will investigate these hypotheses and assess the effect of premature interfacial debonding on the panels' long-term durability.

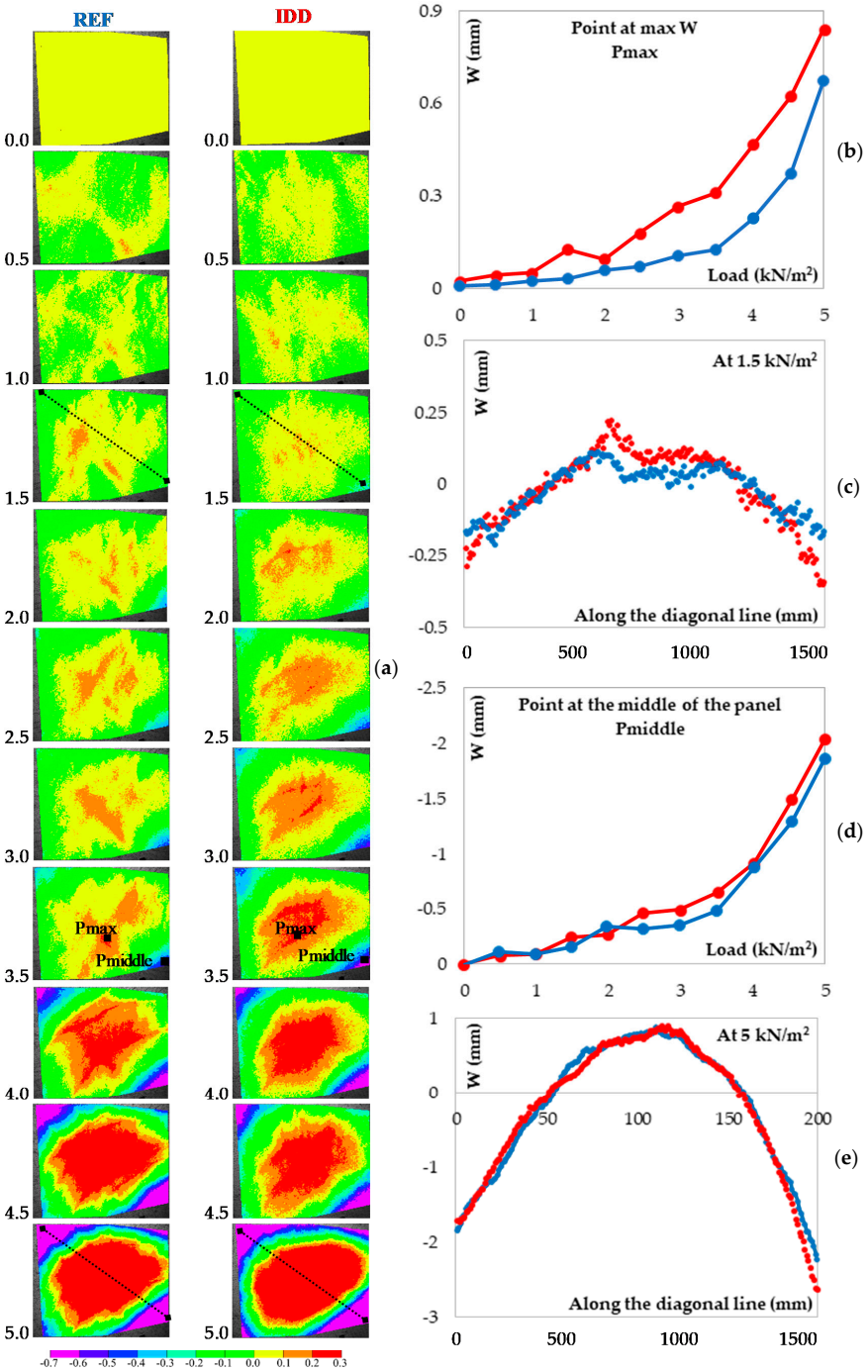

Figure 5. Out-of-plane displacement (mm) (**a**) at each step of incremental load for REF and IID panels, (**b**) at the point of maximum displacement, (**c**) along a diagonal line at 1.5 kN/m^2, (**d**) at the middle of the panel, (**e**) along a diagonal line at 5 kN/m^2.

3.4.3. Extension of Rilem TC 212-ACD Protocol

The Rilem TC 212-ACD protocol has established a methodology to identify the AE source damage mode based on the RA value (RT/amplitude) and the average frequency (AF) trending. Based on this, as the damage mode shifts from mode-I crack opening to shear-dominated and more complex modes, the RA value rises and the AF drops [37]. The protocol is validated for steel rebars-reinforced concrete samples and structural elements and, lately, the research community has been investigating whether these trends are valid for other cement-based materials, fibre/textile reinforced materials, and materials of different dimensions [38,39]. From this perspective, in Figure 6 the RA-AF plots are given, and each point is the average value of the hits detected at the respective load cycle and pause periods. The results are not identical for the two cases under study. In detail, for the REF panel at which damage evolves without the intervention of debonding, there is a clear transition from mode-I crack formation to more complex and shear-oriented damage.

This is an expected result, since at early loading stages the cracks form at the TRC skin. At a moment, specifically at 3.5 kN/m^2, a jump in the RA value is obtained and the AF drops. This is the moment of interfacial debonding, but also of cement extensive cracking and textile activation. The latter is verified by the RA-AF trends that follow, since beyond that point the values of RA-AF are shifted towards shear damage. As proven by the DIC and AE energy/RT analysis above, the interfacial debonding and TRC fracture occur simultaneously until global failure.

On the other hand, no clear trends in the RA-AF averages are obtained for the "debonded series". As illustrated in Figure 6b, there is a clear moment of interfacial debonding at the pause of 1.5 kN/m^2 (15% of ultimate load); once again, this result is validated with the above analyses. The data before and after this moment stand at the same area and cannot be distinguished. This is because of the bad interfacial bonding of the sandwich components, therefore there is shear-dominant AE activity before and after the damage release. Comparing the pre-debonding stage at the REF and IID stage, it is evident that the AF drops and RA value increases in the IID sample; this shift proves the presence of early shear-dominated activity. The Rilem TC 212-ACD protocol highlights the fact that important micro-damage due to shear friction is present as early as at the pause of 0.5 kN/m^2 (5% of ultimate load). This is an essential information for the structural integrity analysis of the panel, and should be correlated to the micro-phenomena that lead to durability loss.

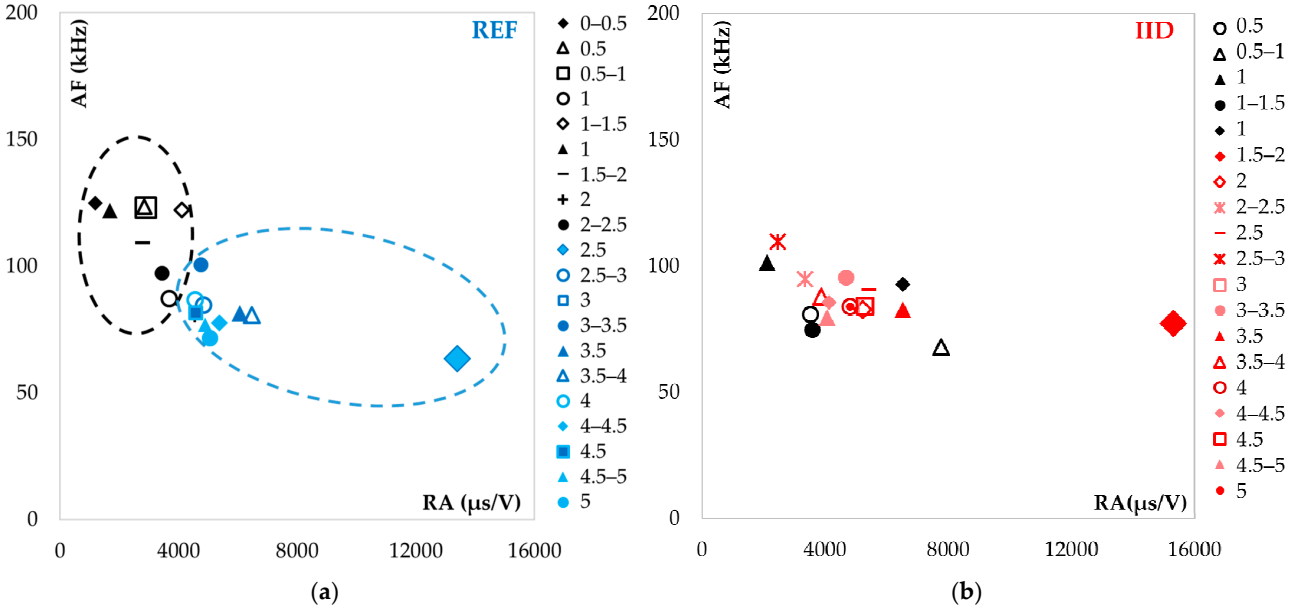

Figure 6. RA value (μs/V)-AF (kHz) average values at each loading step for (**a**) REF and (**b**) IID.

3.4.4. AE Localization Accuracy and the Ability to Predict the Upcoming Failure

In Figure 7, the AE events for the REF panel and throughout the 3.5 kN/m^2 loading cycle are plotted. The black color represents the events that occur as the extra loading is added (it is to be noted that these are part of the first events reported in this test), while the orange dots represent the additional events localized during the pause following this cycle. The AE events initially occur at the middle zone of the sample and progressively cover the area under study. It is also interesting that the orange events (at pause after loading) are located further from the black events, which is evidence that the damage propagates. These results are validated by DIC strain maps at the next loading cycle, where cracks are formed and propagated at the position of AE events. The strain map is projected to correlate with the results of the two methods, although the DIC analysis is conducted at another quartile of the panel. It is proven that AE event localization can predict crack formation and indicate with relevant accuracy the cracking zones; this way, timely inspection can provide an alarm of damage onset and prevention can occur.

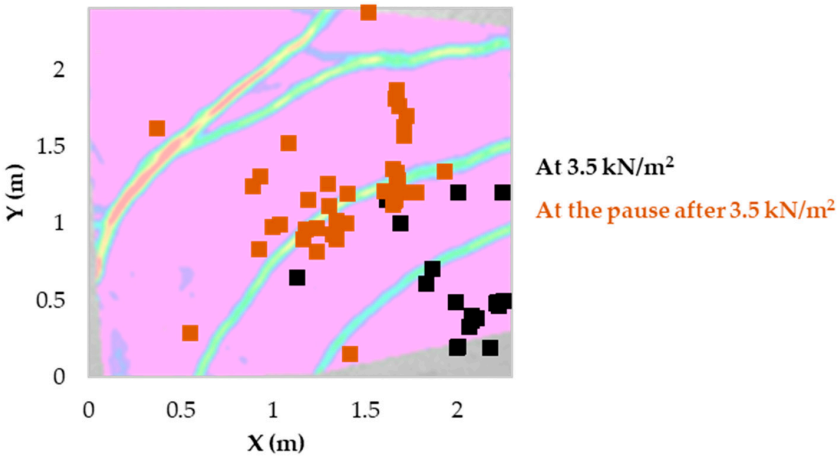

Figure 7. AE events projected at the bottom plane of the TRC skin. In black are the events detected at 3.5 kN/m^2, and in red in Table 1. A strain map at 4 kN/m^2 is projected as a plot background.

4. Conclusions

For the first time in scientific literature, concrete evidence of interfacial debonding on real-size sandwich-insulated panels is tracked by AE and complemented by assessment by DIC. The panels were prepared and cast in an identical way, however they showed intrinsically different early behavior due to the manufacturing disbands (i.e., air pockets), flaws, and defects at the materials' interface. This study proves that the continuous and full-field monitoring of the loading process can detect the premature (as early as at 5% of the ultimate load) detachment of the TRC skin from the core and distinguish this phenomenon from other damage sources that succeed, such as cracking, fiber pull-out, and TRC-textile debonding. Early AE activity is classified as shear-dominated damage (micro-fracture due to friction at the interface) based on RT-IF and RA-AF feature analysis. Out-of-plane displacement mapping can pinpoint the zone, up to 150 mm wide, where local debonding occurs, a result that cannot be obtained based on LVDT or other conventional point-measuring techniques. AE source localization can also localize the internal damaged zones earlier than DIC surface inspection (up to a cycle prior to crack formation); the latter can be a great tool for structural health assessment and prevention actions. From this perspective, this is the first work in the literature that demonstrates a methodology to track damage progress on stratified composite panels with complex fractures. The proposed tools wish to enrich the up-to-date knowledge on insulation panels' premature failure and promote an inspection strategy for the optimal use of materials. This preliminary study should be extended in the future by assessing the efficacy of the proposed methodology for experiments dealing with other types of sandwich-insulated panels—i.e., considering steel

or fibre-reinforced polymer (FRP) skins or using alternative foam core materials such as mineral wool and aerogel.

Author Contributions: Conceptualization, E.T. and M.D.M.; mechanical tests methodology, M.D.M. and H.I.; DIC setup, M.D.M. and H.I.; DIC analysis, AE setup and analysis, E.T.; investigation, M.D.M., H.I., and E.T.; writing—original draft preparation, E.T.; writing—review and editing, M.D.M., D.G.A., T.T., H.I.; funding acquisition, M.D.M. and T.T. All authors have read and agreed to the published version of the manuscript.

Funding: This research was funded by FWO (Fonds Wetenschappelijk Onderzoek-Vlaanderen), grant number 12J7720N. The research of M.D.M. was funded by Agentschap voor Innovatie en Ondernemen (VLAIO) and CRH Structural Concrete Belgium nv (grant number 150251).

Institutional Review Board Statement: Not applicable.

Informed Consent Statement: Not applicable.

Data Availability Statement: The data presented in this study are available on request from the corresponding author.

Conflicts of Interest: The authors declare no conflict of interest. The funders had no role in the design of the study; in the collection, analysis, or interpretation of data; in the writing of the manuscript; or in the decision to publish the results.

References

1. Dey, V.; Zani, G.; Colombo, M.; Di Prisco, M.; Mobasher, B. Flexural impact response of textile-reinforced aerated concrete sandwich panels. *Mater. Des.* **2015**, *86*, 187–197. [CrossRef]
2. Mobasher, B. *Mechanics of Fiber and Textile Reinforced Cement Composites*; CRC Press: Boca Raton, FL, USA, 2011.
3. Mousa, M.A.; Uddin, N. Debonding of composites structural insulated sandwich panels. *J. Reinf. Plast. Compos.* **2010**, *29*, 3380–3391. [CrossRef]
4. Murthy, A.R.; Kumar, V.R.; Gopinath, S.; Prem, R.; Iyer, N.R.; Balakrishnan, R. Structural performance of precast and cast-in-situ ultra-high strength concrete sandwich panel. *Comput. Mater. Contin.* **2014**, *44*, 59–72.
5. Swamy, R.N.; El-Abboud, M.I. Application of ferrocement concept to low cost lightweight concrete sandwich panels. *J. Ferrocem.* **1988**, *18*, 285–292.
6. Cuypers, H. *Analysis and Design of Sandwich Panels with Brittle Matrix Composite Faces for Building Applications*; Vrije Universiteit Brussel (VUB): Brussels, Belgium, 2002.
7. Hegger, J.; Horstmann, M.; Feldmann, M.; Psychny, D.; Raupach, M.; Buttner, T.; Feger, C. Sandwich panels made of TRC and discrete and continuous connectors. In Proceedings of the International RILEM Conference on Material Science, Aachen, Germany, 6–8 September 2010.
8. Shams, A.; Horstmann, M.; Hegger, J. Experimental investigations on Textile-Reinforced Concrete (TRC) sandwich sections. *Compos. Struct.* **2014**, *118*, 643–653. [CrossRef]
9. Shams, A.; Stark, A.; Hoogen, F.; Hegger, J.; Schneider, H. Innovative sandwich structures made of high performance concrete and foamed polyurethane. *Compos. Struct.* **2015**, *121*, 271–279. [CrossRef]
10. O'Hegarty, R.; Kinnane, O. Review of precast concrete sandwich panels and their innovations. *Constr. Build. Mater.* **2020**, *233*, 117145. [CrossRef]
11. Shams, A.; Hegger, J.; Horstmann, M. An analytical model for sandwich panels made of textile-reinforced concrete. *Constr. Build. Mater.* **2014**, *64*, 451–459. [CrossRef]
12. Junes, A.; Larbi, A.S. An experimental and theoretical study of sandwich panels with TRC facings: Use of metallic connectors and TRC stiffeners. *Eng. Struct.* **2016**, *113*, 174–185. [CrossRef]
13. Flansbjer, M.; Portal, N.W.; Vennetti, D.; Mueller, U. Composite behaviour of textile reinforced reactive powder concrete sandwich façade elements. *Int. J. Concr. Struct. Mater.* **2018**, *12*, 1–17. [CrossRef]
14. Mousa, M.A.; Uddin, N. Flexural behavior of full-scale composite structural insulated floor panels. *Adv. Compos. Mater.* **2011**, *20*, 547–567. [CrossRef]
15. de Souza, C.; Barros, J.A.; Correia, J.R.; Valente, T.D. Development of sandwich panels for multi-functional strengthening of RC buildings: Characterization of constituent materials and shear interaction of panel assemblies. *Constr. Build. Mater.* **2021**, *267*, 120849. [CrossRef]
16. Gombeda, M.J.; Naito, C.J.; Quiel, S.E. Development and performance of a ductile shear tie for precast concrete insulated wall panels. *J. Build. Eng.* **2020**, *28*, 101084. [CrossRef]
17. Arevalo, S.; Tomlinson, D. Experimental thermal bowing response of precast concrete insulated wall panels with stiff shear connectors and simple supports. *J. Build. Eng.* **2020**, *30*, 101319. [CrossRef]

18. Kazem, H.; Bunn, W.G.; Seliem, H.M.; Rizkalla, S.H.; Gleich, H. Durability and long-term behavior of FRP/foam shear transfer mechanism for concrete sandwich panels. *Constr. Build. Mater.* **2015**, *98*, 722–734. [CrossRef]
19. Song, F.; Huang, G.L.; Hu, G.K. Online guided wave-based debonding detection in honeycomb sandwich structures. *AIAA J.* **2012**, *50*, 284–293. [CrossRef]
20. Yu, L.; Tian, Z.; Li, X.; Zhu, R.; Huang, G. Core–skin debonding detection in honeycomb sandwich structures through guided wave wavefield analysis. *J. Intell. Mat. Syst. Struct.* **2019**, *30*, 1306–1317. [CrossRef]
21. Tsangouri, E.; Aggelis, D.G. A review of acoustic emission as indicator of reinforcement effectiveness in concrete and cementitious composites. *Constr. Build. Mater.* **2019**, *224*, 198–205. [CrossRef]
22. Yoon, D.J.; Weiss, W.J.; Shah, S. Assessing damage in corroded reinforced concrete using acoustic emission. *J. Eng. Mech.* **2000**, *126*, 273–283. [CrossRef]
23. Carpinteri, A.; Lacidogna, G.; Paggi, M. Acoustic emission monitoring and numerical modeling of FRP delamination in RC beams with non-rectangular cross-section. *Mater. Struct.* **2007**, *40*, 553. [CrossRef]
24. Verbruggen, S.; De Sutter, S.; Iliopoulos, S.; Aggelis, D.G.; Tysmans, T. Experimental structural analysis of hybrid composite-concrete beams by digital image correlation (DIC) and acoustic emission (AE). *J. Nondestruct. Eval.* **2016**, *35*, 2. [CrossRef]
25. Aggelis, D.G.; De Sutter, S.; Verbruggen, S.; Tsangouri, E.; Tysmans, T. Acoustic emission characterization of damage sources of lightweight hybrid concrete beams. *Eng. Fract. Mech.* **2019**, *210*, 181–188. [CrossRef]
26. Abouhussien, A.A.; Hassan, A.A. Acoustic emission monitoring for bond integrity evaluation of reinforced concrete under pull-out tests. *Adv. Struct. Eng.* **2017**, *20*, 1390–1405. [CrossRef]
27. Gallego, A.; Benavent-Climent, A.; Suarez, E. Concrete-galvanized steel pull-out bond assessed by acoustic emission. *J. Mater. Civ. Eng.* **2016**, *28*, 04015109. [CrossRef]
28. Di, B.; Wang, J.; Li, H.; Zheng, J.; Song, G. Investigation of bonding behavior of FRP and steel bars in self-compacting concrete structures using acoustic emission method. *Sensors* **2019**, *19*, 159. [CrossRef]
29. Aggelis, D.G.; Soulioti, D.V.; Sapouridis, N.; Barkoula, N.M.; Paipetis, A.S.; Matikas, T.E. Acoustic emission characterization of the fracture process in fibre reinforced concrete. *Constr. Build. Mater.* **2011**, *25*, 4126–4131. [CrossRef]
30. Li, W.; Ho, S.; Patil, D.; Song, G. Acoustic emission monitoring and finite element analysis of debonding in fiber-reinforced polymer rebar reinforced concrete. *Struct. Health Monit.* **2017**, *16*, 674–681. [CrossRef]
31. Vervloet, J.; Van Itterbeeck, P.; Verbruggen, S.; El Kadi, M.; De Munck, M.; Wastiels, J.; Tysmans, T. Experimental investigation of the buckling behaviour of Textile Reinforced Cement sandwich panels with varying face thickness using Digital Image Correlation. *Constr. Build. Mater.* **2019**, *194*, 24–31. [CrossRef]
32. Fathi, A.; Keller, J.-H.; Altstaedt, V. Full-field shear analyses of sandwich core materials using Digital Image Correlation (DIC). *Compos. B Eng.* **2015**, *70*, 156–166. [CrossRef]
33. De Munck, M.; Tysmans, T.; El Kadi, M.; Wastiels, J.; Vervloet, J.; Kapsalis, P.; Remy, O. Durability of sandwich beams with textile reinforced cementitious composite faces. *Constr. Build. Mater.* **2019**, *229*, 116832. [CrossRef]
34. De Munck, M. *Lomg-Term Performance of a Sandwich Facade System with Textile Reinforced Cementitious Composites*; Vrije Universiteit Brussel (VUB): Brussels, Belgium, 2019.
35. Landis, E.N.; Baillon, L. Experiments to relate acoustic emission energy to fracture energy of concrete. *J. Eng. Mech.* **2002**, *128*, 698–702. [CrossRef]
36. Kravchuk, R.; Landis, E.N. Acoustic emission-based classification of energy dissipation mechanisms during fracture of fiber-reinforced ultra-high-performance concrete. *Constr. Build. Mater.* **2018**, *176*, 531–538. [CrossRef]
37. RILEM Technical Committee. Recommendation of RILEM TC 212-ACD: Acoustic emission and related NDE techniques for crack detection and damage evaluation in concrete. *Mater. Struct.* **2010**, *43*, 1183–1186. [CrossRef]
38. Ospitia, N.; Aggelis, D.G.; Tsangouri, E. Dimension Effects on the Acoustic Behavior of TRC Plates. *Materials* **2020**, *13*, 955. [CrossRef]
39. Zhang, F.; Zarate Garnica, G.I.; Yang, Y.; Lantsoght, E.; Sliedrecht, H. Monitoring Shear Behavior of Prestressed Concrete Bridge Girders Using Acoustic Emission and Digital Image Correlation. *Sensors* **2020**, *20*, 5622. [CrossRef]